LRP 484/93 October 1993

MODE COMPETITION AND STARTUP IN CYLINDRICAL CAVITY GYROTRONS USING HIGH-ORDER OPERATING MODES

D.R. Whaley, M.Q. Tran, T.M. Tran &
T.M Antonsen Jr.

submitted for publication to
5th Special Issue on High Power Microwave of the
IEEE Transactions on Plasma Science

Mode Competition and Startup in Cylindrical Cavity Gyrotrons Using High-Order Operating Modes

D. R. Whaley, M. Q. Tran, T. M. Tran, †T. M. Antonsen Jr.

Centre de Recherches en Physique des Plasmas,
Association Euratom-Confédération Suisse,
Ecole Polytechnique Fédérale de Lausanne, 21 Av. des Bains,
CH-1007 Lausanne, Switzerland

†Laboratory for Plasma Reasearch
and Departments of Electrical Engineering and Physics,
U. of Maryland
College Park, MD 20742

The problem of mode competition in cylindrical cavity gyrotrons is considered. The normalized variable equations are used to calculate the oscillation regions of possible operating modes in the energy - velocity-pitch-angle plane. The analysis is self-consistent and includes the effect of changing beam current, pitch angle, and energy during the startup phase. The time evolution of beam parameters during startup is computed for several types of startup methods and used to determine the oscillating cavity modes during startup. Depending on the type of startup chosen, the cavity can be made to oscillate in several modes or in a single chosen operating mode - even for high order modes where many other possible operating modes exist. Some startup methods are seen to be less favorable than others, allowing for oscillation of unwanted modes and some methods are seen to be more sensitive to small beam/cavity misalignment. The accessibility to the high-efficiency hard excitation region can also be determined and is seen to depend on the startup scenario. The method is general and can be applied to any operating mode with the mode competition analysis specifically useful for high order modes where the spectrum is dense. The analysis of the accessibility to the hard excitation region is applicable to high and low order operating modes. Both $q=1$ and $q=2$ longitudinal mode numbers are considered.

I. Introduction

Gyrotrons operating at high frequency and power require the use of a high-order cavity mode to allow for an increased cavity size and to lower cavity ohmic losses to acceptable levels. The spectrum of modes at such high orders becomes dense and competition between the desired operating mode and nearby modes may become problematic. A gyrotron experiencing severe mode competition may oscillate solely in an unwanted mode for which the frequency can be significantly different than that of the design frequency, the interaction efficiency can be significantly lower than that of the desired operating mode, and line elements and the gyrotron window are mismatched for the new mode. It is therefore important in gyrotron design to assure that monomode operation in the desired operating mode is attainable. For large cavities, designed for operation in a high-order mode, many other modes are capable of oscillating, each with a different quality factor and resonant frequency. To determine which of the possible modes will dominate at the operating point, the beam startup must be considered - the period during which the beam energy, velocity pitch angle, and current are changing before reaching their final operating values[1-5]. If the gyrotron gun design is of triode type, one may specify the relative timing between the voltage rise of the anode and cathode and therefore may control the evolution of beam parameters during the startup. The manner with which one brings these voltages to their nominal values is referred to as a startup scenario. These scenarios can have a large effect on the behavior of the cavity fields during and after the startup portion of the gyrotron pulse. Depending on this time-evolution of the beam parameters, the cavity can be made to oscillate in a single mode[1,2,4] or in many successive modes[3,5] during startup. In some cases, a given startup scenario can be "dangerous" in that it allows for mode competition with modes which couple well to the electron beam. This paper deals specifically with the choice of startup scenarios as it relates to mode competition. The effect of different startup scenarios on the experimental accessibility to the high efficiency region of parameter space

known as the "hard excitation region" is also considered. In Sec. II, the problem of mode competition for a cavity designed to operate at a resonant frequency near $f_{res} = 120GHz$ in the $TE_{22,6}$ mode is presented. The method of calculating the time evolution of the beam parameters during startup is shown in Sec. III as well as the effect of startup on mode competition in the cavity for several specific cases. The sensitivity of the startup cavity fields to misalignment of the beam is also discussed. Results are presented for all first and second longitudinal modes near the desired operating mode. The effect of startup on accessibility to the hard-excitation region is discussed in Section IV. Conclusions are presented in Sec. V.

II. High Order Mode Spectrum and Starting Current

The operating mode of a high frequency, high power gyrotron is chosen to be of high order to limit the loading of the cavity walls to acceptable values. A high order mode ($k_\perp a >> 1$) allows for a large cavity radius and consequently reduced ohmic losses per unit area. Figure 1 shows the cylindrical waveguide $TE_{m,n}$ mode spectrum for modes with $40 < k_\perp a < 50$ where m = *azimuthal mode number* and n = *radial mode number*. Each of the vertical lines represents a possible operating mode with the $TE_{22,6}$ mode found at $k_\perp a = 45.62$. For this paper, the $TE_{22,6}$ mode was chosen as a possible candidate for the operating mode of a high power gyrotron and will be used as an example for all analysis shown. A major disadvantage with choosing a high order mode is that, as seen in Fig. 1, the mode spectrum becomes dense at high values of $k_\perp a$. The cavity is therefore highly overmoded and results in mode competition and in the possibility of oscillation in a mode other than the chosen operating mode. Careful attention must be paid to this problem by considering the coupling of the beam to both the chosen mode and its neighboring modes and by considering the time-dependent behavior of all cavity modes during startup.

To determine, for a given cavity, which modes are possible competitors with the chosen operating mode, one must first determine the resonant frequency and quality factor

for each mode. The quality factor, Q, is defined as $Q = \omega E_{st}/P_{rf}$ where ω = resonant frequency, E_{st} = stored energy, and P_{rf} = output microwave power. All units are MKSA units unless otherwise stated. Many modes are considered as possible competitors to the chosen $TE_{22,6}$ operating mode. All modes with $43 < k_\perp a < 49$ are included (> 60), each mode having its own resonant frequency and quality factor. The values used are cold cavity values with ohmic losses neglected. One can also calculate values of the beam/wave coupling coefficient for the right and left-hand rotating wave of each mode for a beam placed at $r_b/a = 0.52$ where $r_b = beam\ \ radius$ and $a = cavity\ \ radius$. These coupling coefficients, whose expression is shown below, indicate the beam coupling to a given mode in each of the two possible polarizations.

$$C_{mn} = \frac{J^2_{m\pm1}(k_\perp r_b)}{(\nu^2_{mn} - m^2)\ J^2_m(\nu_{mn})}\ , \tag{1}$$

where $k_\perp = \nu_{mn}/a$, $J_m(x) = Bessel\ function\ of\ order\ m$, $\nu_{mn} = n^{th}\ root\ of\ the\ derivative\ of\ the\ Bessel\ function\ of\ order\ m$ — $d(J_m(x))/dx$. If this value is calculated for all modes with $43 < k_\perp a < 49$, one sees that several modes couple as well to the electron beam as the chosen operating mode.

Any gyrotron oscillator can be characterized by three normalized variables representing the cavity electric field, interaction length, and detuning. These unitless values are expressed as[6,7]:

$$F = \frac{E_0\, \beta_\perp^{-3}}{B\ c}\ \ J^2_{m\pm1}(k_\perp r_b)\ , \tag{2a}$$

normalized electric field

$$\mu = \pi \left(\frac{\beta^2_{\perp,}}{\beta_{//}}\right)\left(\frac{L}{\lambda}\right)\ , \tag{2b}$$

normalized interaction length

$$\Delta = \frac{2}{\beta_\perp^{\,2}}\left(1 - \frac{\Omega_{ce}}{\gamma\omega}\right)\ , \tag{2c}$$

detuning

where E_0 = *max electric field in the cavity,* $\beta_\perp = v_\perp/c$, $\beta_\parallel = v_\parallel/c$, B = *magnetic field,* c = *speed of light,* $L = e^{-1}$ *Gaussian width of electric field axial profile,* λ = *freespace wavelength,* Ω_{ce} = *non-relativistic cyclotron frequency,* and γ = *relativistic factor.* Equivalently, the starting current of a mode can be expressed as:

$$I_{st\,A} = 1.68\times10^4 \frac{\gamma I_{st\,N}}{Q} \beta_\perp^4 \frac{L}{\lambda} \frac{(\nu_{mn}^2 - m^2)\, J_m^2(\nu_{mn})}{J_{m\pm1}^2(k_\perp r_b)} , \tag{3a}$$

where

$$I_{st\,N} = \left(\frac{4}{\pi \mu^2}\right)\left[\frac{e^{2x^2}}{\mu x - 1}\right] , \tag{3b}$$

and

$$x = \frac{\mu \Delta}{4} . \tag{3c}$$

Using Eqs. (3), the starting current of each mode considered is calculated. The starting current as a function of detuning is shown in Fig. 2 for operating parameters $E_{beam} = 78keV$, $\alpha = v_\perp/v_\parallel = 1.5$. Modes with $m \geq 0$ are plotted with solid curves and modes with $m < 0$ are plotted with dashed lines. For the detuning which yields high efficiency operation in the $TE_{22,6}$ mode ($\Delta = 0.53$), one sees that many modes have $I_{st} < 20A$ and are therefore capable of oscillating at the operating point with $I_{beam} = 20A$. To determine which of the possible operating modes will dominate at the design point, one must look at the temporal behavior of the cavity modes during the startup phase, where the beam energy, pitch angle, and current are changing before reaching the design point.

III. Startup Scenarios, Mode Oscillation Regions, and Mode Stability

With a triode gyrotron gun, one has separate control over both the anode and cathode voltages allowing for different "startup scenarios" or manners of bringing the operating voltages to their design values. Several examples are shown in Figs. 3-5. The standard

triode startup is shown in Figs. 3 as scenario 1. In this scenario, the full cathode voltage is established before "turning on" the beam by increasing the anode voltage. The relative timing of these voltages is seen in Figs. 3(a)-(c). The evolution of the beam energy and alpha during the beam turn on for any scenario can be calculated using MIG design equations[8]. The anode voltage required to obtain an α for a given beam energy (or equivalently beam γ) is calculated as:

$$V_{anode} = \frac{m_e c^2}{q_e} \frac{\ln(1 + D_F \kappa)}{\ln(1 + 2\kappa)} \left\{ \left[1 + \frac{4}{\kappa^2} \left(\frac{1 + \kappa}{1 + 2\kappa} \right)^2 \left(\frac{\gamma^2 - 1}{R_c^2 \cos^2 \phi_c} \right) \left(\frac{\alpha_0^2}{\alpha_0^2 + 1} \right) \right]^{1/2} - 1 \right\} , \quad (4a)$$

where

$$\kappa = \frac{1}{\sqrt{R_g^2 - 1}} , \quad (4b)$$

$$R_c = \frac{r_c}{r_L} , \quad (4c)$$

$$R_g = \frac{r_{beam}}{r_L} , \quad (4d)$$

$$D_F = \frac{\cos \phi_c}{\kappa} \frac{d_{ac}}{r_c} . \quad (4e)$$

Here, r_L = *cavity Larmor radius* = $\gamma m v_\perp / qB$, d_{ac} = *cathode-anode separation distance*, r_c = *average cathode radius*, γ = *relativistic factor* = $1 + E_{beam}(keV)/511$, ϕ_c = *cathode slant angle*, m_e = *electron mass*, c = *speed of light*, q_e = *electron charge*. To make this calculation, knowledge of the gun design is necessary. Here an example gun design for a $TE_{22,6}$ mode gyrotron is used.

Using Eqs. 4, for a given beam energy, and consequently a given beam γ, the V_{anode} required to obtain a desired beam α can be determined for all α. Then for every point in time during the startup of Figs. 3, the value of α can be determined by interpolation for any combination of ($V_{cathode}$, V_{anode}). In this way the plot of Fig. 3(d), the evolution of α during startup, is determined. Beam α can also be plotted as a function of beam energy as

shown in Fig. 3(e) and for this triode-like startup scenario appears as a straight vertical line in the (α, E_{beam}) plane. The evolution of α for other possible startup scenarios is also computed and shown in Figs. 4 and 5. Scenario 2 of Fig. 4 is a simulated diode-like startup where both the cathode and anode voltages are increased simultaneously to their full operating voltages. The α *vs.* E_{beam} plot of Fig. 4(e) is seen to be substantially different from that of the triode-like startup scenario 1 of Fig. 3(e). Paths in the (α, E_{beam}) plane lying between scenario 1 and scenario 2 are also possible by changing the timing of the start of the V_{anode} rise. Scenario 3 of Figs. 5 is one example. Scenario 4 is a scenario in which the anode and cathode voltages are first brought independently to values close to their nominal final values but always remaining low enough so that, as will be seen later, no cavity modes will be excited. Then after these intermediate voltages have been established, the final rise to full voltages occurs together. This results in a path in the (α, E_{beam}) plane shown as scenario 4 in Fig. 5(e) which has certain advantages to be seen later. The final startup scenario 5 is similar to that of scenario 4 except that the anode voltage is immediately brought to full value after an intermediate cathode voltage has been established. This eliminates the need for precise relative timing of the anode and cathode voltages. The path of this scenario is also seen in the (α, E_{beam}) plane of Fig. 5(e).

In general, during the startup phase of a cavity several modes will oscillate as the beam α and energy change. To determine when the $TE_{22,6}$ will begin oscillating during any of the scenarios 1-5, the starting current, I_{st}, is calculated for all values of α and E_{beam}, for $0.5 < \alpha < 2.5$ and $50keV < E_{beam} < 90keV$, using Eqs. 3, and the contours for $I_{st} < 50A$ are plotted in Fig. 6(a). In this plot as well as those of Figs. 7 and 8, the $I_{st} = 20A$ line is plotted in bold as it is for a beam with parameters near this line that the chosen mode will begin to oscillate assuming a final beam current of $I_b = 20A$. The beam lines for the scenarios of Figs. 3-5 can now be superimposed on the plot of Fig. 6(a). At any point then during the startup, one can determine the starting current of any mode from plots similar to that of Fig. 6(a). Another startup line is shown in Fig. 6(a) as the bold dashed line near the line for startup scenario 2. This is the true diode startup line. In this case, no startup scenario is required since α is a function of E_{beam} assuming $v_\perp \propto V_{cathode}$,

$E_{beam} = qV_{cathode}$, and imposing $\alpha = 1.5$ at $E_{beam} = 78keV$. This beam line is seen to be similar to that of startup scenario 2. These starting current contours are plotted for two other troublesome modes in Figs. 6(b) and (c). Fig. 6(b) is for the $TE_{21,6}$ mode which has the minimum starting current of all modes at the operation point, as seen in Fig. 2, and Fig. 6(c) is for the $TE_{.19,7}$ which is close in frequency to the $TE_{22,6}$ mode and which has a coupling coefficient comparable to that of the $TE_{22,6}$ mode. Each of these curves will be considered shortly.

The effect of changing beam current during the startup phase must now be accounted for in the same (α, E_{beam}) parameter range as in Fig. 6(a). Using Eqs. 4, for each value of E_{beam} (or γ), the anode voltage V_{anode}, required to attain a desired α is calculated for all α. In this way, Fig. 7 is generated as the contours of the anode voltage required to reach the particular point in the (α, E_{beam}) plane. For the gun design in this example gyrotron, an anode voltage of $V_{anode} \sim 24.5kV$ is seen to be the final anode voltage required to attain the design beam α of $\alpha = 1.5$ for a beam energy of $E_{beam} = 78keV$.

Using the Richardson-Dushman equation for electron emission from a hot cathode in the presence of an electric field[9], the values of $V_{anode} = f(\alpha, E_{beam})$ of Fig. 7 are used to compute the beam current for the same range of α and E_{beam} as Figs. 6(a) and 7.

$$J\left(\frac{A}{m^2}\right) = J_0 \; exp\left(\frac{0.44}{T}\sqrt{\frac{V_{anode}}{d_{ac}}}\right) , \tag{5a}$$

where

$$J_0\left(\frac{A}{m^2}\right) = 1.2\times10^6 \, T^2 \; exp\left(-\frac{11600}{T}\phi\right) , \tag{5b}$$

and T = *cathode temperature* in K, and ϕ = *work function of cathode material in eV*, and d_{ac} = *anode-cathode separation distance*. Here, the cathode temperature is chosen to give exactly the design current of $I_b = 20A$ at the design values of α, E_{beam}, V_{anode} taken from Fig. 7. The beam current is therefore calculated as:

$$I_{beam} = I_{op} \; exp\left(\frac{0.44}{T\sqrt{d_{ac}}}\left[\sqrt{V_{anode}} - \sqrt{V_{anode\ op}}\right]\right) , \tag{6}$$

where I_{op} is the design operating current in A and T is the solution of:

$$\ln T + \frac{1}{T}\left(0.22\sqrt{\frac{V_{anode\ op}}{d_{ac}}} - 11600\ \frac{\phi(eV)}{2}\right) + \frac{1}{2}\ln\left(\frac{1.2\times10^{6}\,A_c}{I_{op}}\right) = 0\ , \qquad (7)$$

where A_c = *cathode emitting area in* m^2. Equation 7 is easily solved numerically and is generally on the order of $T = 1100\text{-}1300K$. Using Eqs. 6 and 7 and the $V_{anode} = f(\alpha, E_{beam})$ values of Fig. 7, the beam current for every point in the (α, E_{beam}) plane can be calculated and the contours are shown in Fig. 8. The same beam paths of scenarios 1-5 as shown in Figs. 6(a) and 7 are included in Fig. 8. Since it was seen that the region of interest for the $TE_{22,6}$ mode lies above the bold U-shaped line on the figures, it is seen that regardless of the beam path taken, the beam current is typically within *10-15%* of its final value when it reaches the point where the mode will oscillate. The beam power, however, may be as low as 70% of its value at the nominal operating voltages. It should be noted that of the three sets of contour plots of Figs. 6(a), 7, and 8, only Fig. 6(a) is mode dependent. The V_{anode} and I_{beam} contours are valid for all cases with similar gun designs.

The starting current contours of Fig. 6(a) and the beam current contours of Fig. 8 are now combined to self-consistently determine where during startup, the $TE_{22,6}$ mode will begin oscillating. The curve marked *22,6* on Fig. 9(a) is the locus of points in the (α, E_{beam}) plane where the starting current from Fig. 6(a) and the beam current from Fig. 8 are equal. Inside the U-shaped curve, $I_{beam} > I_{st}$ and outside the curve $I_{beam} < I_{st}$. In this way it becomes clear at which point during the startup that the $TE_{22,6}$ will start *if* it is the only mode available to oscillate at the point in the (α, E_{beam}) plane where the beam line crosses the locus line. Whether this is true, depends on the startup scenario chosen and the beam line that is followed. A similar calculation is performed for the $TE_{21,6}$ mode of Fig. 6(b) and its locus line is plotted on Fig. 9(a) with that of the $TE_{22,6}$ mode.

Considering the locus lines of Fig. 9(a) and the possible startup paths, it immediately becomes clear which startup scenarios are preferable from the point of view of mode competition between the $TE_{22,6}$ and the $TE_{21,6}$ modes. During startup scenario 1, the

oscillation regions of the two modes are entered at approximately the same time. There is therefore a significant risk that the unwanted $TE_{21,6}$ mode will begin oscillating before the desired operating mode. If, however, the diode-like scenario 2 is chosen, the oscillation region of the $TE_{22,6}$ mode is entered well before that of the $TE_{21,6}$ and the risk of oscillation in the $TE_{21,6}$ is eliminated. Therefore, it is evident that the choice of startup scenario is important to insure startup in the desired mode.

The stability of a mode is also of importance. If an operating mode is stable, a parasitic mode will not grow in the presence of the operating mode, *even* if the operation point lies in the oscillation region of the parasitic mode - i.e. oscillation with a stable operating mode raises the starting currents of all other nearby modes to such an extent that they will never start in the presence of the stable mode. The stability of the operating mode depends on the beam parameters and can change from stable to unstable as one moves in the (α, E_{beam}) plane. The best operating mode will be stable everywhere within its operation region - stable against growth of all other parasitic modes for all points in the oscillation region. A multimode code[10] is used to determine the stability region of the $TE_{22,6}$ mode and is shown as the cross-hatched region in Fig. 9(a). In this case, for all values of $\alpha < 1.6$, the $TE_{22,6}$ mode is stable within the entire oscillation region. Therefore, once the $TE_{22,6}$ mode begins oscillating it will remain the dominant mode for as long as the beam path remains within the $TE_{22,6}$ oscillation region.

Another effect is clear from Fig. 9(a). If for example, the diode-like startup path is chosen, care must be taken not to "overshoot" the operating point. The point of optimum efficiency is always located far to the right side of the oscillation region in the (α, E_{beam}) plane. This means that if the beam line continues past the operating point by even a small amount, there is a risk that oscillation in the main mode will cease allowing for another mode, the mode with the minimum starting current at the present beam conditions, to begin oscillating. It should be noted that the filling time, $Q/\omega \sim 10ns$, is considerably shorter than ramp time scales and the equilibrium states can be considered as established instantaneously. This effect will be present for any mode which lies in a dense part of the mode spectrum and sets an upper limit on the amount of overshoot which can be tolerated in the power supplies

controlling V_{anode} and $V_{cathode}$. This must be considered in the design of the gyrotron regulator and modulator.

Considering now mode competition between the $TE_{22,6}$ and the $TE_{-19,7}$, Fig. 9(b) shows the locus lines for these modes, computed from Figs. 6(a) and (c) and Fig. 8. Competition with mode $TE_{-19,7}$ is seen to be of concern since the locus line of the $TE_{-19,7}$ is close to that of the $TE_{22,6}$ for all paths of entry into the oscillating region of the $TE_{22,6}$. It is however seen that ideally the $TE_{-19,7}$ should not be excited for any of the startup scenarios chosen since the startup path crosses the locus line of the $TE_{22,6}$ mode before that of the $TE_{-19,7}$ mode for all startup paths. The beam position of $r_b/a = 0.52$ was chosen partially to decouple the beam from the $TE_{-19,7}$ mode as much as possible without significantly decreasing the coupling to the $TE_{22,6}$ mode. The effect of small errors in the beam placement can now be examined. Fig. 9(b) is now regenerated for a beam located at $r_b/a = 0.47$ and shown in Fig. 9(c). The effect is immediately visible. The locus line of the $TE_{-19,7}$ no longer lies completely inside that of the $TE_{22,6}$ mode. This means that certain startup scenarios are more sensitive to small changes in beam position than others. Here, the most insensitive startup scenario is seen to be that of the diode-like startup scenario 2. The other startup scenarios 1, 3, 4, 5 are more sensitive to beam position and the allowable error in beam position will be smaller than that for startup scenario 2. In this sense the diode startup scenario is the "safest" from the point of view of mode competition with respect to beam displacement.

To have a comprehensive overview of the problem of mode competition during startup, the locus lines for all considered modes have been computed and superimposed. This is shown in Fig. 10 for $r_b/a = 0.52$ as well as the beam lines for startup scenarios 1-5. The modes may be identified in a similar method to that of Fig. 2. Here it is seen that modes well separated in frequency from the desired operating mode can be excited during the startup. In this figure, all modes with radial mode number $n = 6$ have been plotted in bold. This includes from left to right in the figure, mode $TE_{24,6}$, $TE_{23,6}$, $TE_{22,6}$, $TE_{21,6}$. It is immediately clear how scenarios 3, 4 and 5 will behave. Since the $TE_{22,6}$ locus line is crossed first and the mode is stable within its oscillation region, it will be the

first mode to start and will remain the oscillating mode during the rest of the startup, up to and including the operation point. During these startup scenarios, unlike those of scenario 2 and the real diode scenario, no mode other than the desired operating mode will oscillate in the cavity. Scenario 1 has been seen to be unacceptable, as the $TE_{21,6}$ mode risks starting before the $TE_{22,6}$ mode at the point where the scenario 1 beam path crosses the locus lines of the two modes at the same time. The diode-like scenario 2 is seen to cross the locus lines of many modes during startup. Starting at the far left of the figure on the beam path of scenario 2, it is seen that the $TE_{23,6}$ mode is first excited (after skimming the $TE_{22,6}$ and $TE_{.21,7}$ locus lines). It then continues to oscillate throughout its oscillation region. Though it is not clear exactly where the $TE_{23,6}$ will cease to oscillate when it has reached the right side of its oscillation region, it is seen through multimode simulations[10] that it is indeed near the locus line of the mode where the oscillations begin to damp. For the $TE_{23,6}$ mode, this occurs near $\alpha = 1.1$, $E_{beam} = 62keV$. At this point the $TE_{23,6}$ mode damps allowing for another mode to grow. Any mode which includes the point $\alpha = 1.1$, $E_{beam} = 62keV$, in its oscillating region is capable of oscillating and will compete with the other possible modes. At the point $\alpha = 1.1$, $E_{beam} = 62keV$, this is seen to include eight other modes. Multimode simulations show that of the possible modes, the one which has the minimum starting current at the point of interest generally is the mode to dominate. Though it is not completely clear from Fig. 10 which mode of the eight possible modes has a minimum starting current at this point, it is true that points located the furthest vertically from the locus line and points displaced to the left in the oscillating region have the lowest starting current. In this case it is the next azimuthal mode, the $TE_{22,6}$ mode, which will dominate at the point where the $TE_{23,6}$ starts to damp and the $TE_{22,6}$ mode will continue to be the dominant mode up to the operating point since it has been seen to be stable against growth of parasitic modes for its entire oscillation region.

From Fig. 10, it is seen that all startup scenarios except the triode-like startup scenario 1 will result in monomode operation in the $TE_{22,6}$ mode. Scenarios 3, 4, and 5 result in a startup where only the desired operating mode is present in the cavity during the entire startup. These startup scenarios, though, have been seen to be sensitive to beam

placement. The diode-like startup scenario 2 is the least sensitive to errors in beam placement but it relies on "jumping" from one azimuthal mode to the next during the startup until the desired operating mode is reached. It is also the scenario the most sensitive to overshoot, too great a value of which will cause a jump to another operating mode, which may continue to oscillate suppressing the $TE_{22,6}$ mode even once the beam returns to its design operating point. Scenario 4 has the advantage that the anode and cathode voltages can be brought up near to their final operating values, while always remaining out of the region of oscillation. Any noise, overshoot, etc., on the voltages caused by the rapid rise from zero to near full voltage will have no effect on the startup. Then the short path between the "elbow" on the path of scenario 4 to the operating point can be performed in a carefully controlled manner, avoiding any transients seen to be particularly dangerous. This though requires reasonably precise timing for the rise of the anode and cathode voltages. Precise timing, however, is not required for the path of scenario 5. The problem of overshoot during the initial rise of the cathode and anode voltages using this scenario is alleviated also. As seen in the locus plots, though, scenario 5 results in a portion of the startup where $\alpha_{beam} > \alpha_{final}$. This may result in reflection of a portion of the beam if α is allowed to rise too high before turning toward the operation point.

The plots of Figs. 6-10 consider only modes with longitudinal mode number $q = 1$. There is a concern that competition may exist between higher order longitudinal modes, the primary concern being the $q = 2$ modes. Therefore the cold cavity resonant frequencies and quality factors for all modes near $TE_{22,6}$ for $q = 2$ are regenerated. It is seen that the quality factors for these modes are about a factor of 5-6 below those of the $q = 1$ modes. To generate the starting current for these modes, one can no longer use the Gaussian approximation used in the derivation of Eqs. 3. Here one must use a sinusoidal approximation and the expressions for the starting current becomes[11]:

$$I_{st\,A} = \frac{4\gamma \varepsilon_0 m_e}{q_e} \frac{\omega}{Q} |p_0|^2 \frac{k_{\parallel}^2 v_{\parallel}^2}{J_{m\pm1}^2(k_{\perp} r_b)} \left[s\beta_{\perp}^2 \frac{dF_c}{dx} - 2F_c \right]^{-1}, \qquad (8a)$$

where

$$|p_o|^2 = \frac{\pi L}{2}\frac{1}{k_\perp^2}(\nu_{mn}^2 - m^2)\, J_m^2(\nu_{mn}) \quad ,$$

$$k_{\parallel} = \frac{q\pi}{L} \quad ,$$

$$F_c = \frac{2}{(1-x^2)^2}\sin^2\left[\frac{(x+1)\,q\pi}{2}\right] \quad , \tag{8b}$$

$$x = \frac{\Omega_c/\gamma - \omega}{k_{\parallel}\, v_{\parallel}} \quad , \quad s = \frac{\Omega_c/\gamma}{k_{\parallel}\, v_{\parallel}} \quad .$$

Here q = *longitudinal mode number*, m_e = *electron mass*, q_e = *electron charge*. Figure 11 shows the starting currents as a function of magnetic field for all modes of Fig. 2 but for $q = 2$. Here the starting current for all modes has been conservatively divided by the constant factor required to match the $q = 1$ minimum starting current for Gaussian and sinusoidal assumption of the fields. Again for the magnetic field of interest, it is seen that several modes, including the $TE_{22,6}$ $q = 2$ mode, can oscillate. To determine if these modes can be competitive with the $TE_{22,6}$ $q = 1$ mode, the locus plots for the modes near the $TE_{22,6}$ mode are regenerated and plotted in Fig. 12. These curves could be directly superimposed on the plot of Fig. 10 and it is seen from Fig. 10 that by the time the beam reaches the oscillation region of any of the $q = 2$ modes, the $q = 1$ modes are well established and almost to their nominal operating point. Therefore problems are not expected with mode competition for $q = 2$ modes.

IV. Accessibility to Hard Excitation Region

The problem of choosing a startup scenario as it relates to access to the hard excitation region is now considered. For the example cavity used in this paper, the beam/wave interaction efficiency for the $TE_{22,6}$ mode as a function of detuning Δ (defined by Eq. (2c)) is computed and shown in Fig. 13. This is a non-linear, self-consistent, hot cavity computation[12] and is performed by varying the applied magnetic field for constant E_{beam} and α. The points on the plot can be divided into three different groups. The points marked

with a filled circles are stable equilibrium points in the soft excitation region. These points are accessible experimentally regardless of which startup path of Sec. III is chosen. The points marked with open circles are stable equilibrium points in the hard excitation region. Accessibility to these points depends on the startup scenario. The points marked with crosses are unstable equilibrium points and therefore can never be attained experimentally but serve to show the division between the soft and hard excitation regions. In general, to attain operation at points in the hard excitation region, one must approach the operating point with increasing beam detuning. From the specific example of Fig. 13, it is seen that to access the hard excitation region points, the detuning, sometime during the pulse must cross $\Delta = 0.46$ from below before reaching its final value at $\Delta = 0.53$. It is desirable to operate in the hard excitation region because, as is seen in the figure, the efficiency increases by ~5% as one moves from the soft to the hard excitation region. It also insures high power operation in the case of significant power reflection back into the cavity due to impedance mismatch. One must now determine the time evolution of the detuning values for each of the startup scenarios 1-5 (with scenarios 3 and 4 changed somewhat for the purpose of illustration). This is done on the same (E_{beam},α) plane that was used to calculate the oscillation regions of the competing cavity modes. For every (E_{beam},α) pair the detuning can be computed for a given magnetic field. These contours are then plotted in Fig. 14(a) as well as the startup paths shown on Fig. 10. From Fig. 14(a) it is clear which startup scenarios allow access to the hard excitation region. Any scenario which crosses the $\Delta = 0.46$ contour sometime during its path will allow access to the high efficiency region. In Fig. 14(a), the $\Delta = 0$ contour is seen to be vertical and lie at $E_{beam} = 51keV$ for all α. This implies that if the cathode voltage remains below $V_{cathode}$ ~$50kV$ at the time when the anode voltage begins to rise, that the detuning as a function of time will increase from zero past $\Delta = 0.46$ and onto the operating Δ value of $\Delta = 0.53$. Other scenarios are also possible. For scenarios 1-5, if the values of detuning shown on the paths of Fig. 14(a) are plotted, one can see the time variation of detuning with each scenario chosen. The triode scenario 1 is seen to be a monotonically decreasing function of time and therefore cannot operate in the hard excitation region. Scenarios 4 and 5 are in principle acceptable because,

though they start at a high value of detuning, they decrease below the threshold value of $\Delta = 0.46$ before rising again to the final value of $\Delta = 0.53$. Scenarios 2 and 3 are seen to be the safest scenarios to assure access to the hard excitation region as they are monotonically increasing functions of time which increase directly from $\Delta = 0$ to $\Delta = 0.53$.

V. Conclusions

A method has been presented to analyze mode competition in cylindrical cavity gyrotrons. The method considers the time-evolution of the electron beam of the gyrotron during the startup phase and self-consistently accounts for changing beam energy, alpha and current before the beam reaches its final operating point. Oscillation regions for each possible cavity mode are computed and used to determine when during startup a given mode will begin oscillating. Stability of the operating mode in its operating region of parameter space is also computed and used to assure no growth of parasitic modes in the presence of the operating mode. With a gyrotron triode gun, the manner with which the beam is started is seen to strongly affect the cavity wave fields during the startup portion of the pulse and in some cases determines the final dominant mode. Longitudinal mode competition can also be analyzed and for a typical cavity the first longitudinal mode is seen to be well established, regardless of the startup scenario, before reaching the oscillation region of the second longitudinal mode. Access to the high efficiency hard excitation region is seen to be dependent on the startup scenario also. A typical triode startup, where the cathode voltage is established at its nominal value before raising the anode voltage, will not reach the hard excitation region and is seen to decrease the attainable efficiency by ~5%. A diode-type startup, however, where the cathode and anode voltages are raised simultaneously is seen to allow access to the hard excitation region thereby increasing the attainable efficiency by ~5%. Other startup scenarios are also possible. A stepped startup scenario, with an intermediate cathode voltage of $V_{cathode} \sim 50kV$ appears to be the most favorable. This

scenario allows access to the hard excitation region and assures that only the desired operating mode is present in the cavity during the entire startup. It is also one of the scenarios the least sensitive to errors in beam position. Finally, it is seen that regardless of the startup scenario, overshoot in the cathode and anode voltages must be carefully controlled in order to assure continued operation in the desired operating mode.

Acknowledgments

This work was partially supported by the Fonds National Suisse pour la Recherche Scientifique. The authors would also like to acknowledge fruitful discussions with Dr. T. P. Goodman of the CRPP, Drs. E. Borie, G. Gatenbein, and Prof. M. Thumm of the Kernforschungszentrum, Karlsruhe, Drs. A. Dubrovin and P. Garin of Thomson Tubes Electroniques and Dr. A. Goldenberg of IAP Nizhny Novgorod.

Mode Competition and Startup in Cylindrical Cavity Gyrotrons Using High-Order Operating Modes

References

1.) G. S. Nusinovich, "Methods of Voltage Feeding Providing Single-mode, Highly Efficient Operation in Pulsed Gyrotrons", *Elektronnaya Tekhnika,* Ser.I, Elektronika SVCh, 44-49, 1974.

2.) E. Borie and B. Jodicke, "Start-up and mode competition in a 150 GHz gyrotron", *Int. J. Infrared and Millimeter Waves*, **8** 207-226, 1987.

3.) B. Levush and T. M. Antonsen Jr., "Mode competition and control in high power gyrotron oscillators", *IEEE Trans. Plasma Sci.*, **18** 260-272, 1990.

4.) O. Dumbrajs and G. S. Nusinovich, "Theory of a Frequency-Step-Tunable Gyrotron for Optimum Plasma ECRH", *IEEE Trans. Plasma Sci.*, **20**, 452-457, 1992.

5.) E. Borie, G. Gatenbein, B. Jödicke, G. Dammertz, O. Dumbrajs, T. Geist, G. Hochschild, M. Kuntze, H.-U. Nickel, B. Piosczyk and M. Thumm, *Int. J. Electron.* **72**, 687 (1992).

6.) B. G. Danly and R. J. Temkin, *Phys. Fluids* **29**, 561 (1986).

7.) K. E. Kreischer, B. G. Danly, J. B. Schutkeker, and R. J. Temkin, "The Design of Megawatt Gyrotrons", *IEEE Trans. Plasma Science*, Vol. PS-13 No. 6, pp. 364-373, 1985.

8.) J. M. Baird and W. Lawson, *Int. J. Electron.* **61**, 953 (1986).

9.) S. Humphries, *Charged Particle Beams* (John Wiley & Sons, New York, 1990).

10.) S. Y. Cai, T. M. Antonsen, Jr., G. Saraph and B. Levush, *Int. J. Electron.* **72**, 759 (1992).

11.) K. E. Kreischer and R. J. Temkin, *Infrared and Millimeter Waves*, Vol. 7, pp. 377-485, 1983.

12.) P. Muggli, M. Q. Tran, T. M. Tran, H.-G. Mathews, G. Agosti, S. Alberti, and A. Perrenoud, "Effect of Power Reflection on the Operation of a Low-Q Gyrotron", *IEEE Trans. on Mirowave Theory and Techniques*, **38** 1345-1351, 1990.

Mode Competition and Startup in Cylindrical Cavity Gyrotrons Using High-Order Operating Modes

Figure captions

Figure 1. Mode spectrum for TE modes in cylindrical waveguide for $40 < k_{\perp}a < 50$.

Figure 2. Starting current curves of modes near mode $TE_{21,6}$ with a mode identification table shown to the right of the plot. The bold curve is the starting current curve for the $TE_{22,6}$ mode. Beam parameters are $\alpha = 1.5$, $E_{beam} = 78keV$, $r_b/a = 0.52$.

Figure 3. Startup scenario 1 - typical triode startup - anode voltage rises after full cathode voltage is established. Time traces of (a) cathode + anode voltage (b) beam α and (c) beam α vs. beam energy.

Figure 4. Startup scenario 2 - typical diode startup - anode and cathode voltages rise together. Time traces of (a) cathode + anode voltage (b) beam α and (c) beam α vs. beam energy.

Figure 5. Startup scenarios 3, 4, 5. (a) time trace of cathode + anode voltage for startup where anode voltage rises only after the start of the cathode voltage rise (b) time trace of cathode + anode voltage for stepped startup where intermediate anode and cathode voltages are established before making the final rise together to the full nominal voltage values (c) time trace of cathode + anode voltage for stepped startup scenario where an intermediate cathode voltage is established before the full anode voltage is applied. The cathode voltage then rises to it's nominal value at full anode voltage (d) time trace of beam α for previous scenarios and (e) beam α vs. beam energy for previous scenarios.

Figure 6. Starting current contours as a function of beam α and beam energy E_{beam} for (a) the $TE_{22,6}$ mode (b) the $TE_{21,6}$ mode (c) the $TE_{-19,7}$ mode and $r_b/a = 0.52$. The paths of the five startup scenarios of Figs. 3-5 are shown in bold as well as the diode startup scenario.

Figure 7. Contours of anode voltage as a function of beam α and beam energy E_{beam}. The bold U-shaped curve is the $I_b = 20A$ starting current contour of Fig. 6(a). The various startup scenarios are also shown in bold.

Figure 8. Contours of beam current as a function of beam α and beam energy E_{beam}. The bold U-shaped curve is the $I_b = 20A$ starting current contour of Fig. 6(a). The various startup scenarios are also shown in bold.

Figure 9. Locus lines for (a) $TE_{22,6}$ and $TE_{21,6}$ modes at $r_b/a = 0.52$, (b) $TE_{21,6}$ and $TE_{-19,7}$ modes at $r_b/a = 0.52$ (c) $TE_{22,6}$ and $TE_{-19,7}$ modes at $r_b/a = 0.47$ as a function of beam α and beam energy E_{beam}. The various startup scenarios are also shown in bold.

Figure 10. Locus lines in the (α, E_{beam}) plane for all modes near $TE_{22,6}$ at $r_b/a = 0.52$. The various startup scenarios are also shown in bold.

Figure 11. Second longitudinal mode starting current curves for modes near mode $TE_{21,6}$ with a mode identification table shown to the right of the plot. The bold curve is the starting current curve for the $TE_{22,6}$ mode. Beam parameters are $\alpha = 1.5$, $E_{beam} = 78keV$, $r_b/a = 0.52$.

Figure 12. Second longitudinal mode locus lines in the (α, E_{beam}) plane for all modes near $TE_{22,6}$ at $r_b/a = 0.52$. The various startup scenarios are also shown in bold.

Figure 13. Computed electronic interaction efficiency vs. detuning for $I_b = 20A$. (filled circles) stable soft-excitation region points (open circles) stable hard-excitation region points (crosses) unstable operating points.

Figure 14. (a) Detuning contours in the (α, E_{beam}) plane with the various startup scenarios shown in bold (b) detuning vs. time for scenarios 1-5.

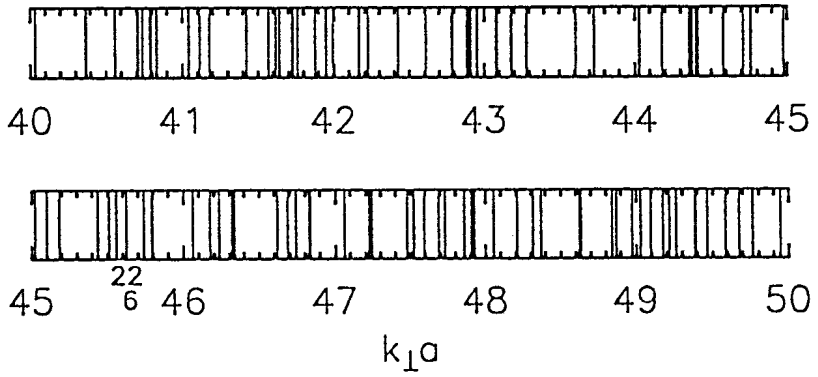

Figure 1

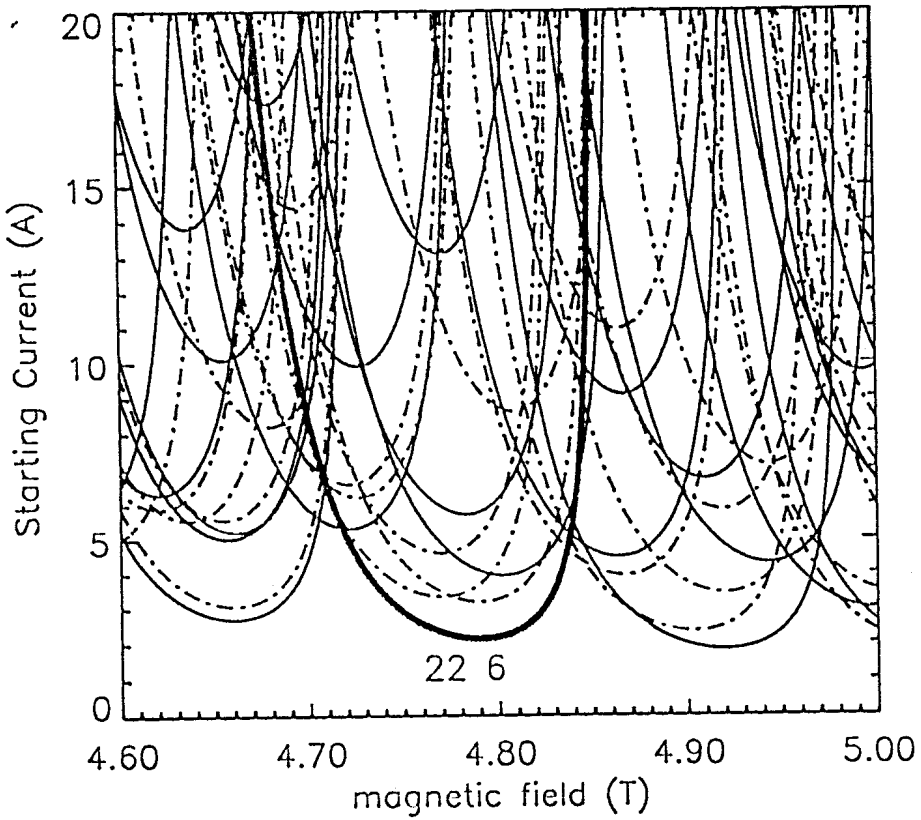
20
15
10
5
0
Starting Current (A)
22 6
4.60
4.70
4.80
4.90
5.00
magnetic field (T)

Figure 2

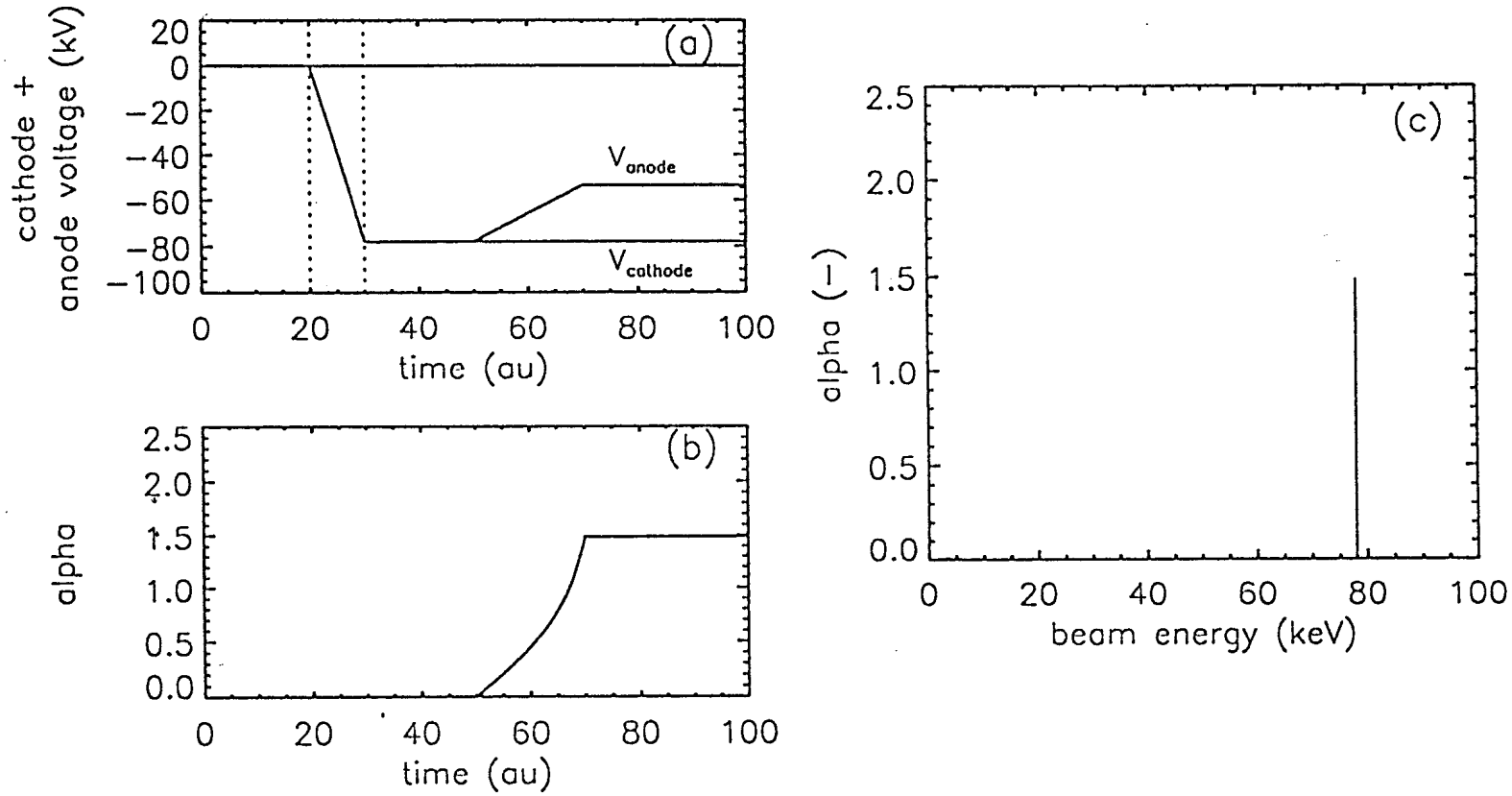
cathode + anode voltage (kV)
20
0
−20
−40
−60
−80
−100
(a)
V_{anode}
$V_{cathode}$
0
20
40
60
80
100
time (au)
alpha
2.5
2.0
1.5
1.0
0.5
0.0
(b)
0
20
40
60
80
100
time (au)
alpha (−)
2.5
2.0
1.5
1.0
0.5
0.0
(c)
0
20
40
60
80
100
beam energy (keV)

Figure 3

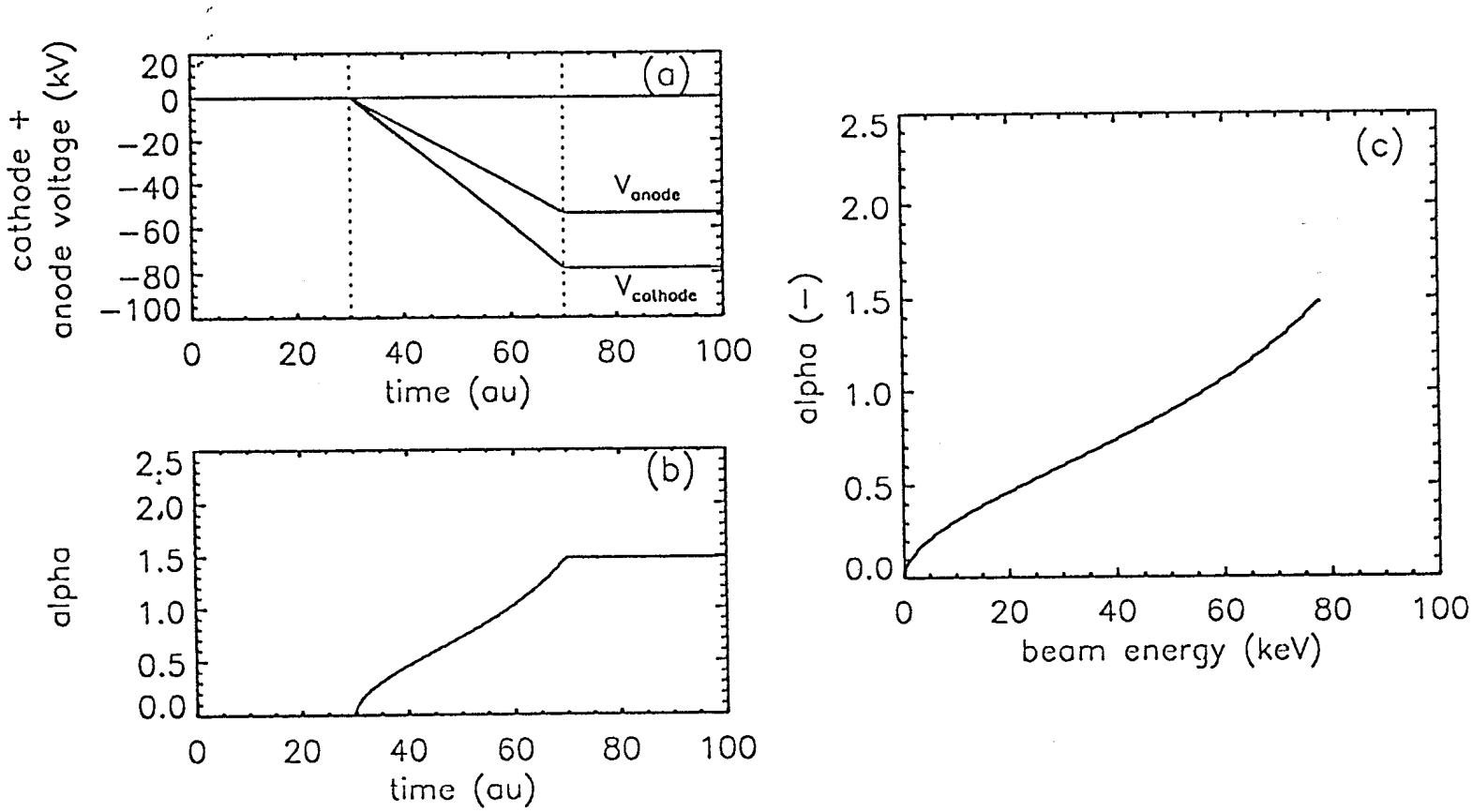
cathode + anode voltage (kV)
20
0
−20
−40
−60
−80
−100
(a)
V_{anode}
$V_{cathode}$
0
20
40
60
80
100
time (au)
alpha
2.5
2.0
1.5
1.0
0.5
0.0
(b)
0
20
40
60
80
100
time (au)
alpha (−)
2.5
2.0
1.5
1.0
0.5
0.0
(c)
0
20
40
60
80
100
beam energy (keV)

Figure 4

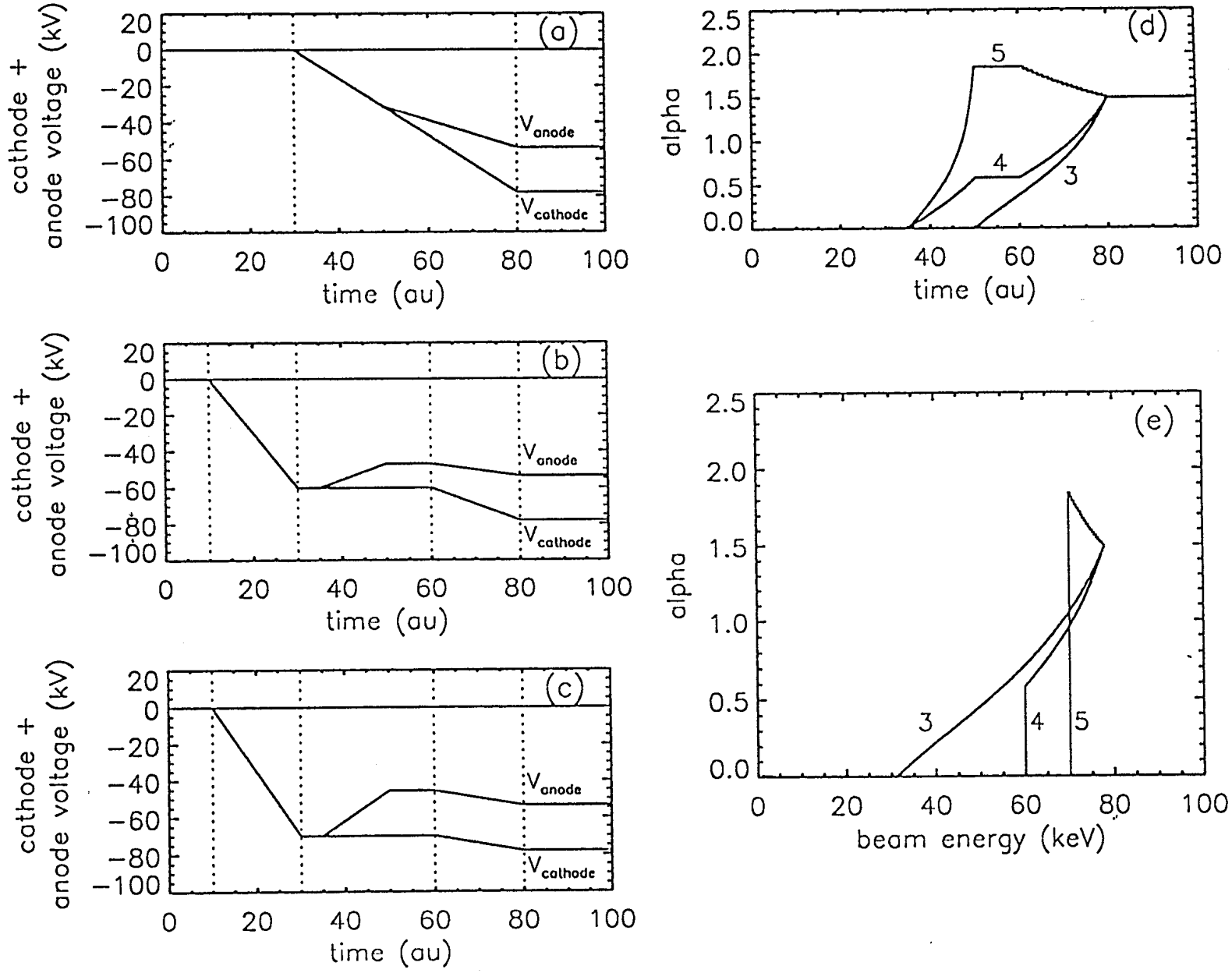
(a)
(b)
(c)
(d)
(e)
cathode + anode voltage (kV)
time (au)
V_{anode}
$V_{cathode}$
alpha
beam energy (keV)
3
4
5

Figure 5

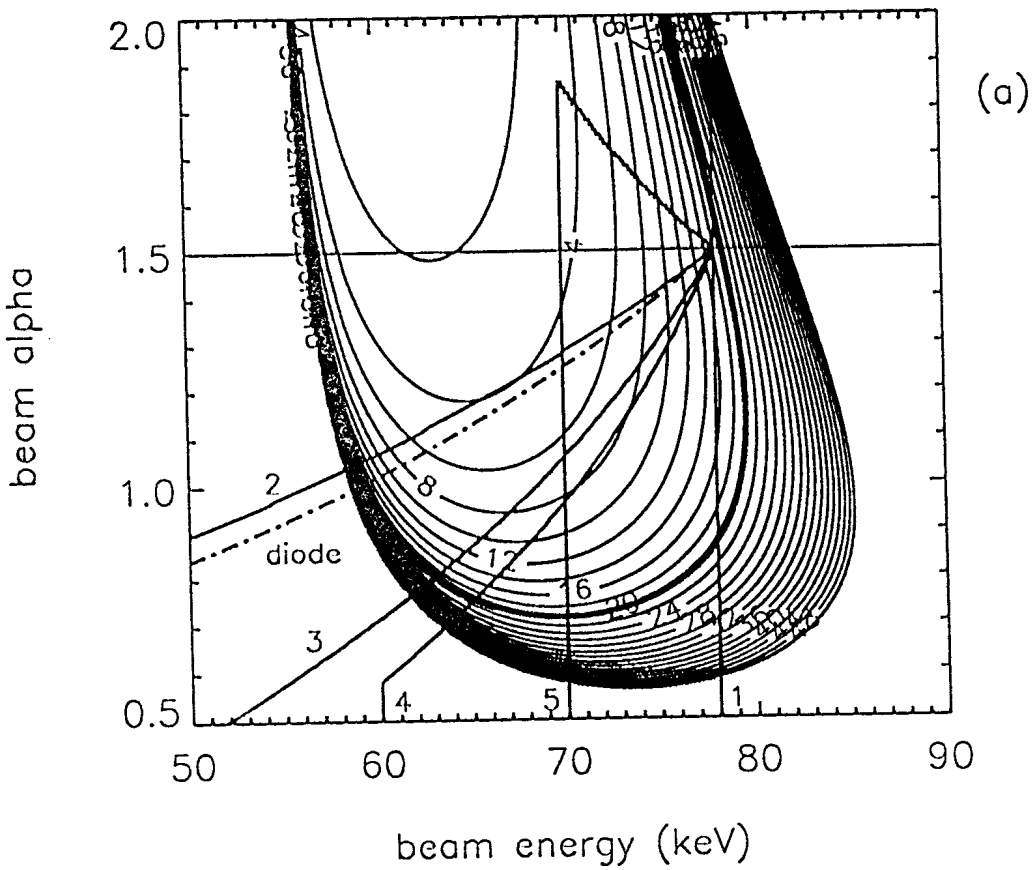
2.0
1.5
1.0
0.5
beam alpha
50
60
70
80
90
beam energy (keV)
(a)
diode
1
2
3
4
5
6
8
12
20
74

Figure 6(a)

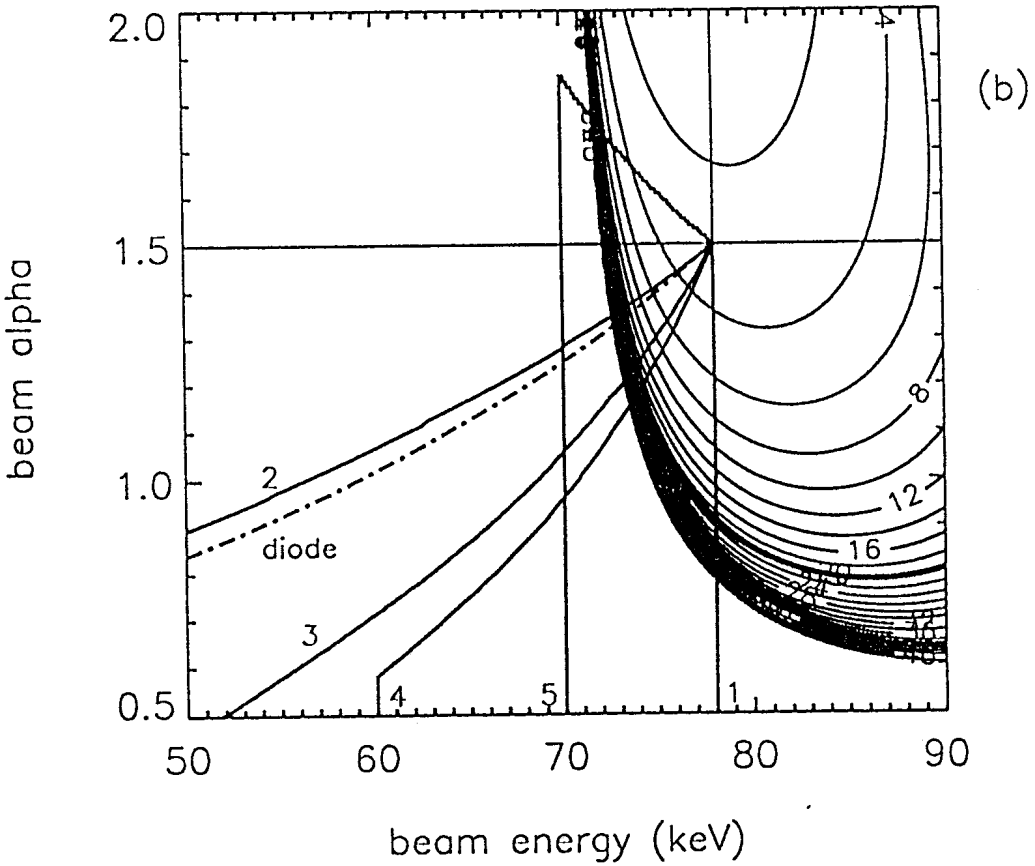
2.0
1.5
1.0
0.5
beam alpha
50
60
70
80
90
beam energy (keV)
(b)
2
diode
3
4
5
1
8
12
16

Figure 6(b)

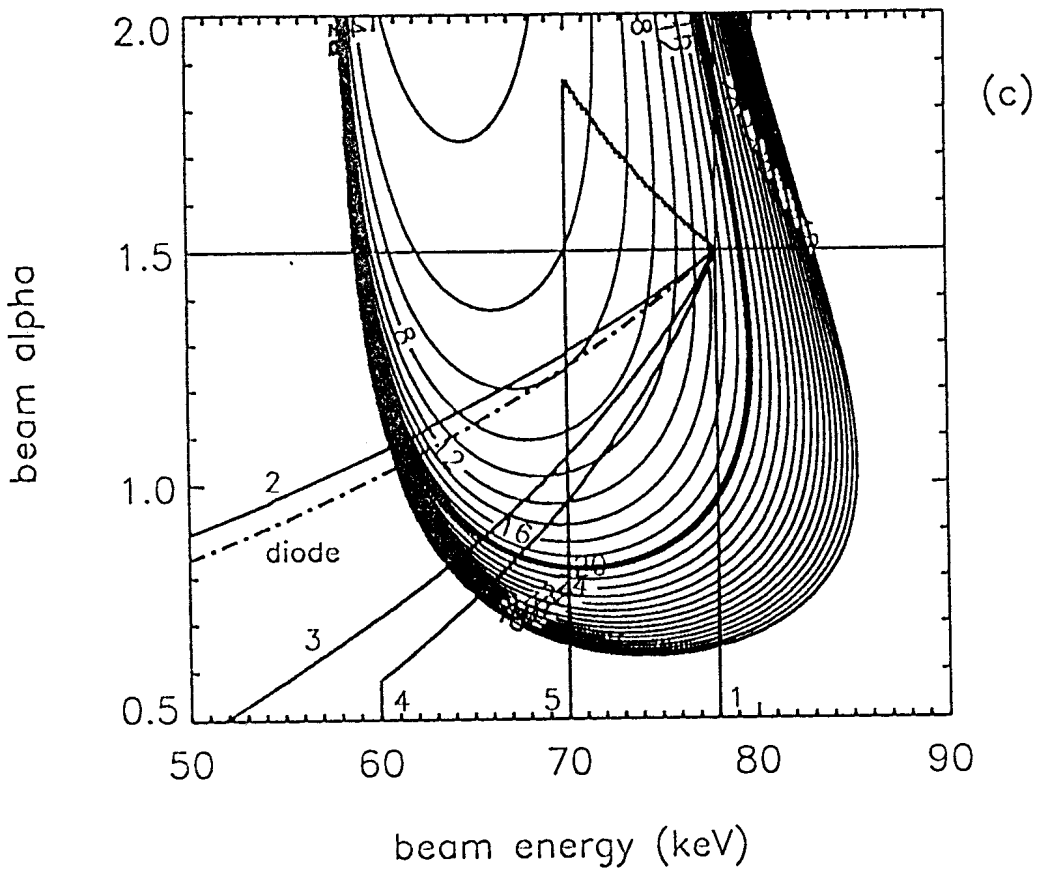
2.0
1.5
1.0
0.5
beam alpha
50
60
70
80
90
beam energy (keV)
(c)
diode
1
2
3
4
5
8
12
16
20
24

Figure 6(c)

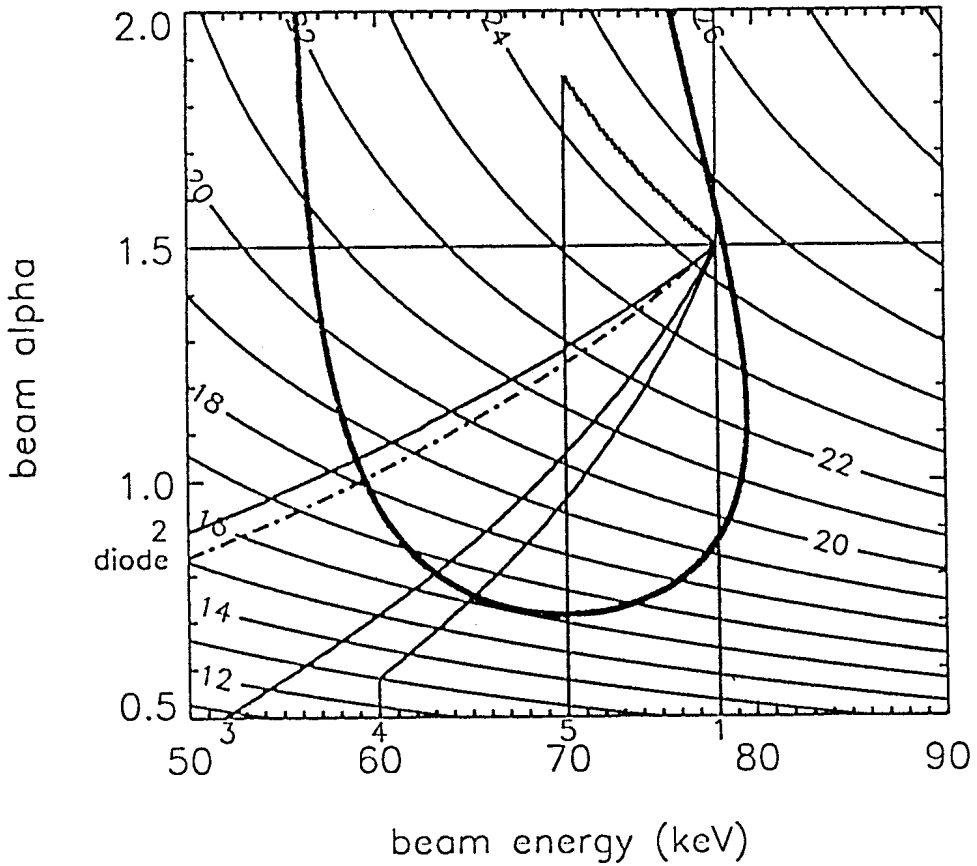
2.0
1.5
1.0
0.5
beam alpha
diode
2
3
4
5
1
50
60
70
80
90
beam energy (keV)
26
24
28
30
18
16
14
12
22
20

Figure 7

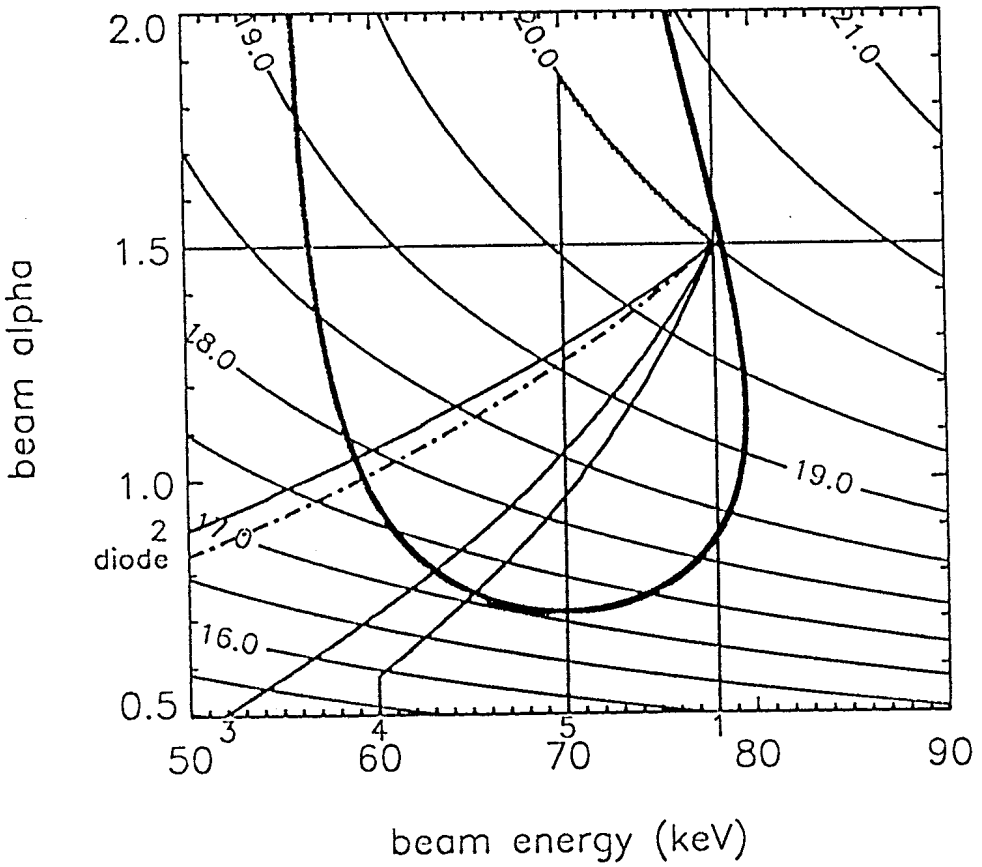
2.0
1.5
1.0
0.5
beam alpha
19.0
20.0
21.0
18.0
19.0
17.0
2
diode
16.0
3
4
5
1
50
60
70
80
90
beam energy (keV)

Figure 8

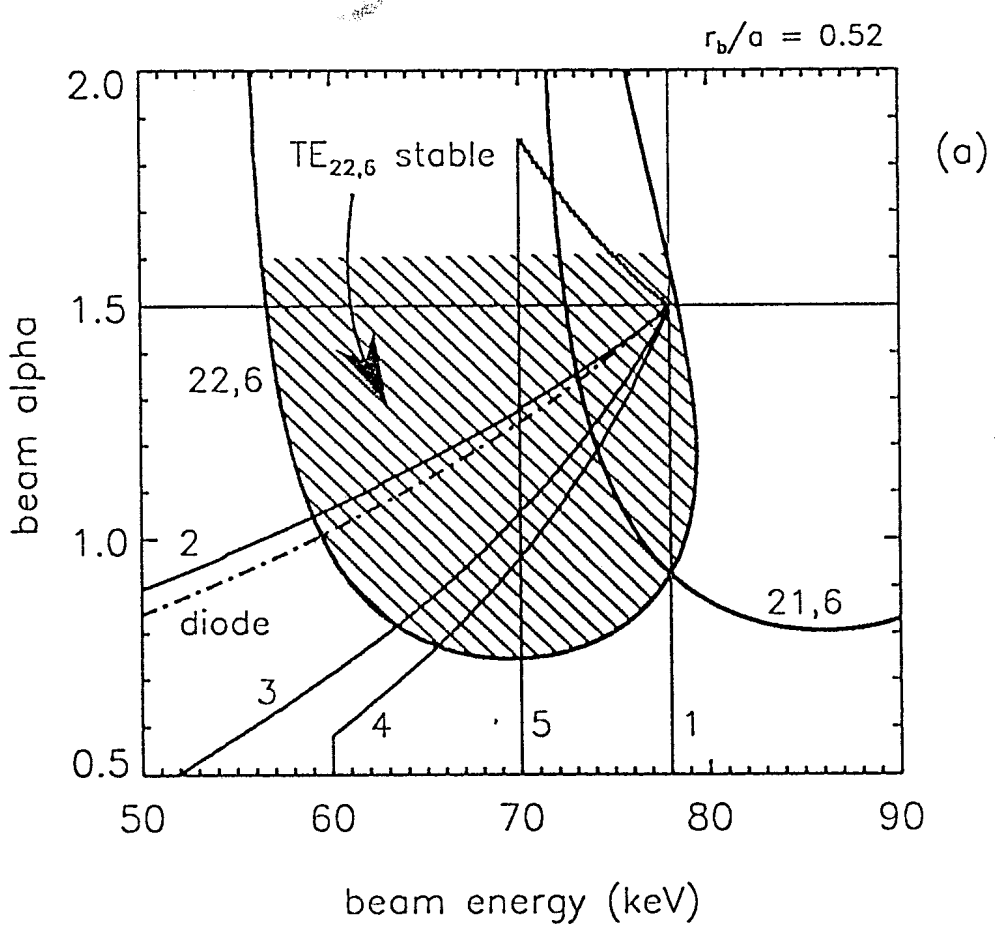
r_b/a = 0.52
(a)
$TE_{22,6}$ stable
22,6
2
diode
3
4
5
1
21,6
2.0
1.5
1.0
0.5
beam alpha
50
60
70
80
90
beam energy (keV)

Figure 9(a)

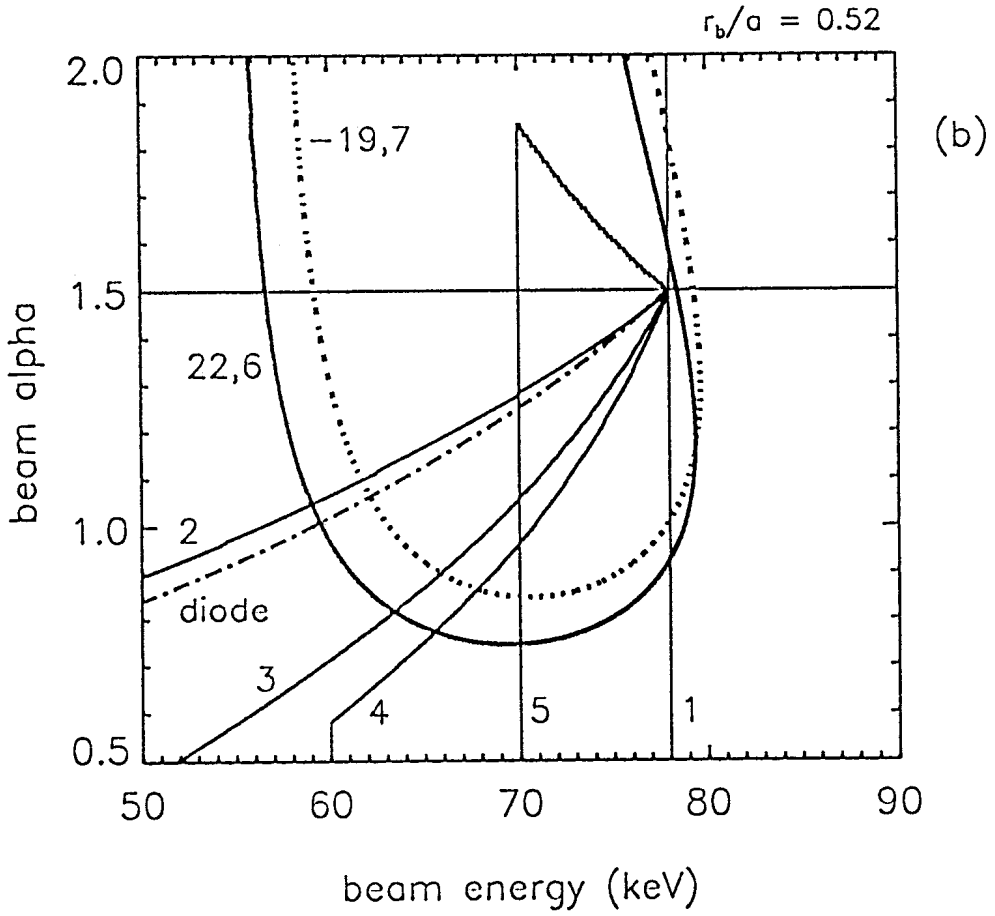
r_b/a = 0.52
(b)
2.0
1.5
1.0
0.5
beam alpha
−19,7
22,6
2
diode
3
4
5
1
50
60
70
80
90
beam energy (keV)

Figure 9(b)

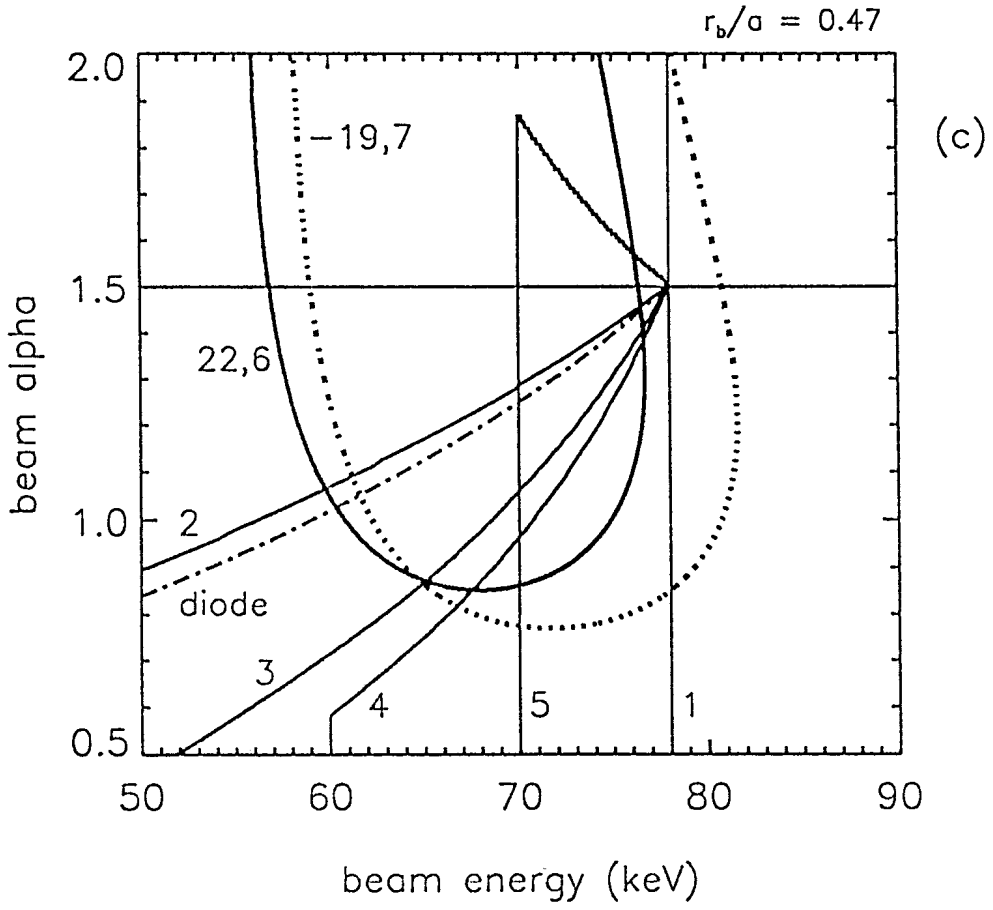
r_b/a = 0.47
(c)
2.0
1.5
1.0
0.5
beam alpha
−19,7
22,6
2
diode
3
4
5
1
50
60
70
80
90
beam energy (keV)

Figure 9(c)

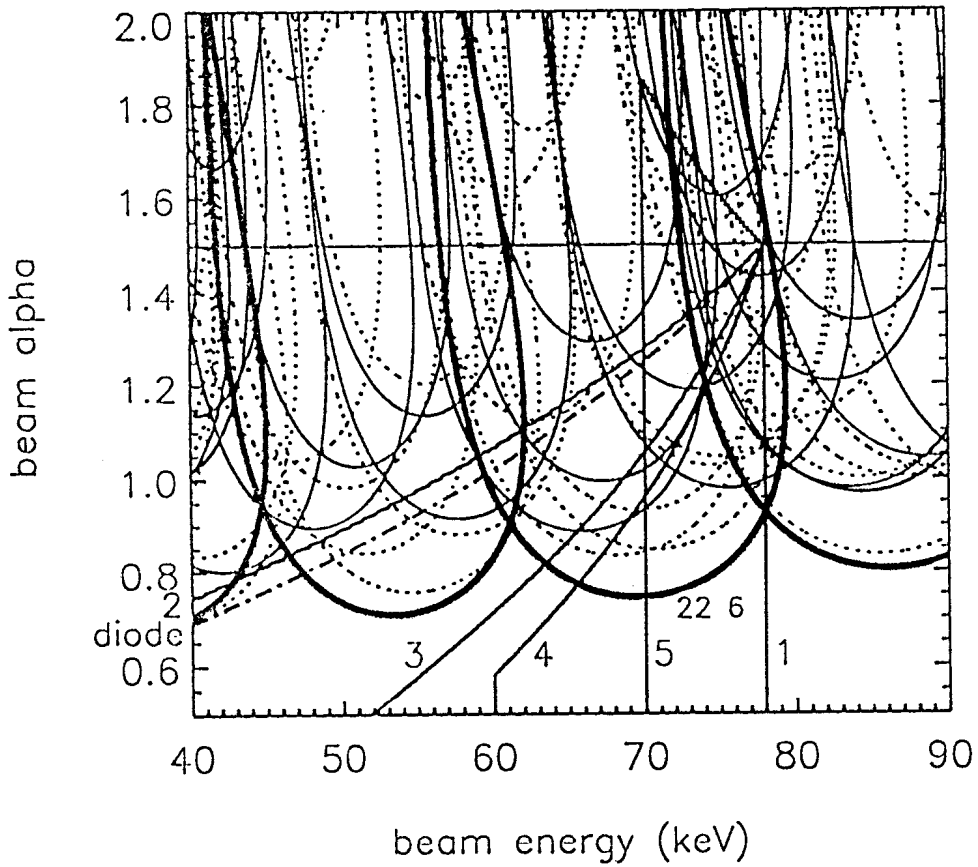
2.0
1.8
1.6
1.4
1.2
1.0
0.8
0.6
beam alpha
2
diode
3
4
5
22 6
1
40
50
60
70
80
90
beam energy (keV)

Figure 10

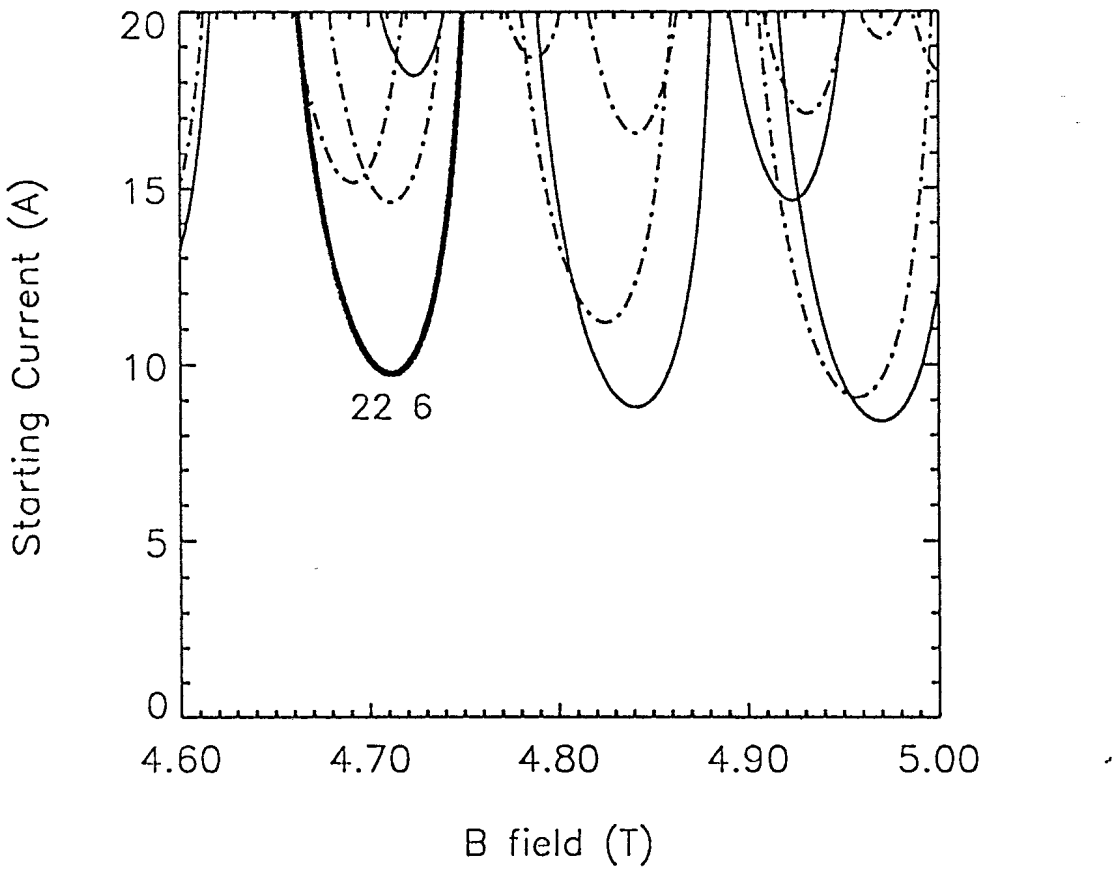

Figure 11

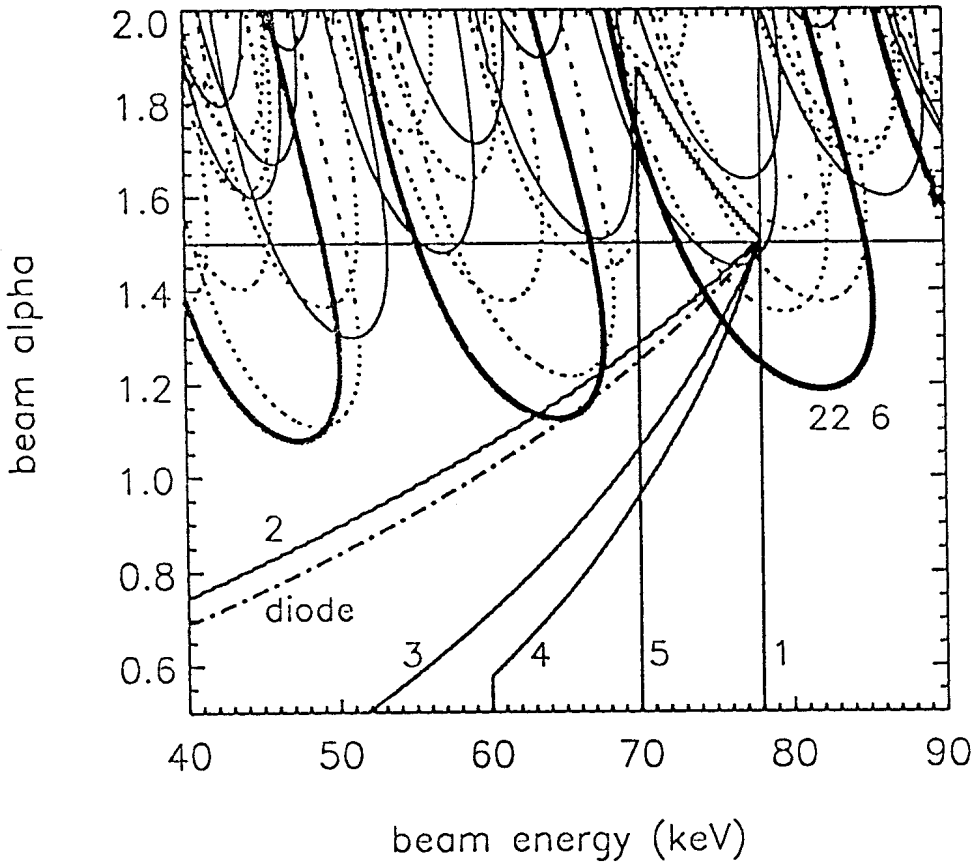
2.0
1.8
1.6
1.4
1.2
1.0
0.8
0.6
beam alpha
40
50
60
70
80
90
beam energy (keV)
22 6
2
diode
3
4
5
1

Figure 12

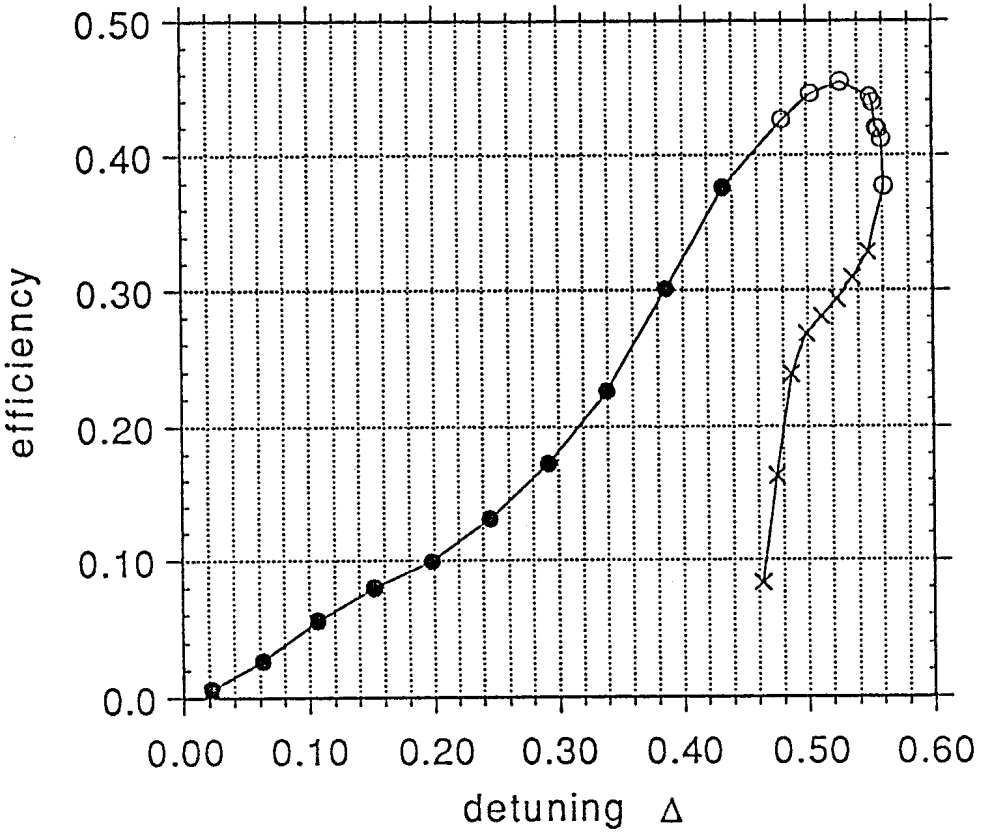
0.50
0.40
0.30
0.20
0.10
0.0
efficiency
0.00
0.10
0.20
0.30
0.40
0.50
0.60
detuning Δ

Figure 13

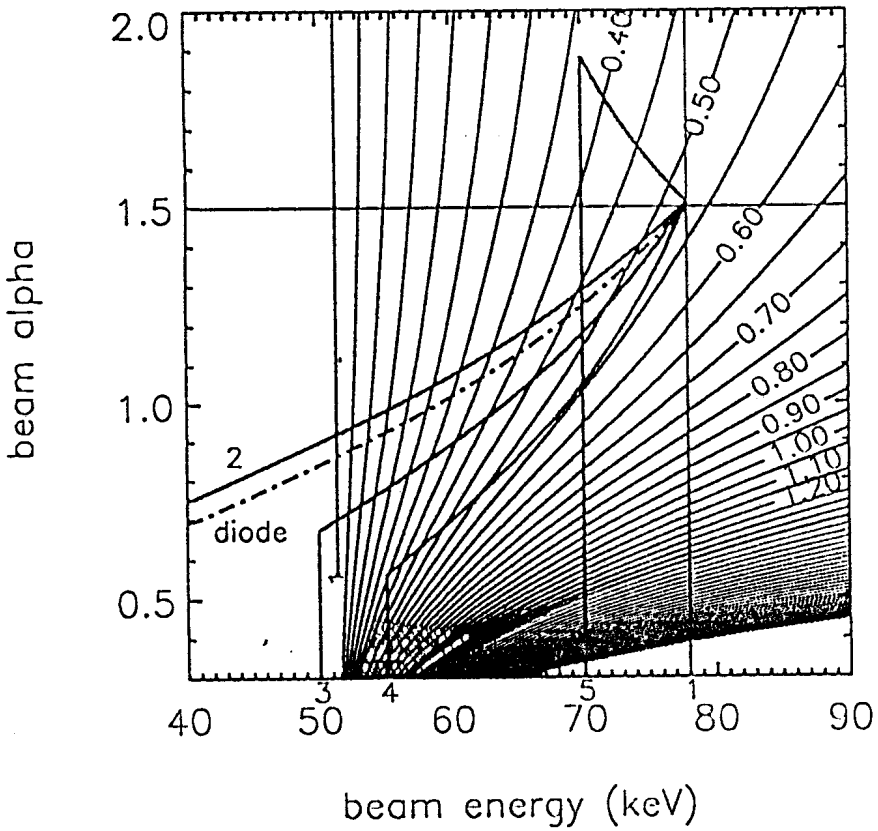

Figure 14(a)

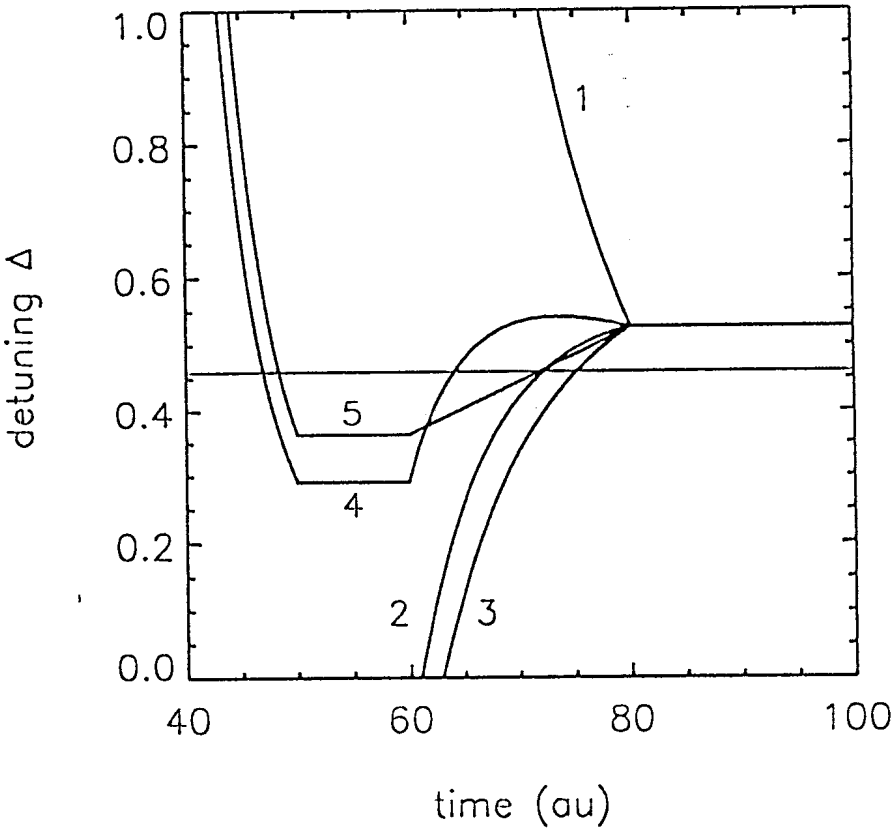

Figure 14(b)